Digital filtering: a common analysis for data and mean field theories

J-F. Lecolley[1], E. Galichet[2], D.C.R. Guinet[2], R. Bougault[1], F. Gulminelli[1].
G. Auger[3], Ch-O. Bacri[4], F. Bocage[1], B. Borderie[4],
R. Brou[1], P. Buchet[5], J-L. Charvet[5], A. Chbihi[3], J. Colin[1],
D. Cussol[1], R. Dayras[5], A. Demeyer[2], D. Doré[5], D. Durand[1],
J.D. Frankland[4], E. Genouin-Duhamel[1], E. Gerlic[2], P. Lautesse[2],
J-L. Laville[3], T. Lefort[1], R. Legrain[5], N. LeNeindre[1], O. Lopez[1], M. Louvel[1],
A-M. Maskay[2], L. Nalpas[5], A.D. Nguyen[1], M. Parlog[6], J. Péter[1],
E. Plagnol[4], M-F.Rivet[4], E. Rosato[7], F. Saint-Laurent[3], J-C. Steckmeyer[1],
M. Stern[2], G. Tabacaru[6], B. Tamain[1], L. Tassan-Got[4], O. Tirel[3],
E. Vient[1], C. Volant[5] and J-P. Wieleczko[3].
[1]LPC, IN2P3-CNRS et Université, 14050 Caen Cedex, France.
[2]IPN Lyon, IN2P3-CNRS et Université, 69622 Villeurbanne, Cedex, France.
[3]GANIL, CEA et IN2P3-CNRS, B.P. 5027, 14076 Caen Cedex, France.
[4]IPN Orsay, IN2P3-CNRS, 91406 Orsay Cedex, France.
[5]DAPNIA/SPhN, CEA/Saclay, 91191 Gif-sur-Yvette Cedex, France.
[6]Nuclear Inst. for Physics and Nuclear Engineering, Bucharest, Roumania.
[7]Dipartimento di Scienze, Univ. Di Napoli, 80125 Napoli, Italy.

19th January 1999

Abstract

To select well-defined event configurations from heavy ion collisions in the Fermi energy domain, a digital filtering technique of the charge density distribution along the deflection axis in the velocity space is presented. Charge density appears as a robust variable and can be used for a quantitative comparison of experimental data obtained with 4π arrays and mean field transport equation predictions.

1 Introduction

Multiple fragment and particle production is the dominant feature of heavy ion induced reactions in the Fermi energy domain. Using 4π-multiparticle detection, we have to manipulate *many-body* observables. Global variables have been developed in particle physics to characterize with few numbers the high multiplicity events. In nuclear physics they are used not only to obtain information on the event shape, but also as impact parameter selectors. Composite fragments production, finite particle numbers and multiplicity fluctuations are shown to have important effects [1] on the event-shape analysis. A precise event shape determination using global variable techniques is limited by the difficulty to achieve a correct weighting of composite fragments with respect to light particles. The global variables used to classify roughly the events according to the violence of the collision are often constructed with a portion of the event, either the light particles or the fragments. The boundary between these two categories may be ambiguous, especially for medium size systems. Moreover, an event shape analysis does not allow to sort out the different exit channels corresponding to a given impact parameter. The actual event configuration clearly results from the convolution of fluctuations in the interaction phase and of several decay modes in the exit channel, therefore an experimental determination of the impact parameter may depend upon some combination of these variables.
Even after impact parameter selection, the comparison of experimental data with one-body semi-classical transport models is not obvious to achieve. In these models only density distributions in phase space are defined and the fragment formation is not addressed. To get rid of multiplicity fluctuations, we propose to construct the charge density distribution along the deflection axis of the di-nuclear system formed in the exit channel of a heavy ion reaction. This distribution is expressed as a development in Hermite polynomials [2]. Using some specific properties of the development coefficients, it is easy to select well-defined event configurations.
The set of data obtained with the INDRA detector on a medium size system ($^{36}Ar +^{58} Ni$ in the 32-95 A.MeV bombarding energy range) has been used to test this technique.

2 Data sample pre-requirements

A global visualization of many body events can only be accomplished if a maximum of information is collected on an event by event basis. This general consideration has led us to test the proposed analysis technique on a "well detected" sample recorded with the INDRA 4π detector. The chosen system is $^{36}Ar+^{58}Ni$ in the 32-95 A.MeV bombarding energy range. Only those events fulfilling a recorded pseudo parallel linear momentum ($P_{detected} = \Sigma_i Z_i\, V_{i//}$) greater than 80 % of the incident one have been retained as "well detected" events.
A detailed description of the 4π INDRA detector, together with charge identification and calibration procedures, can be found elsewhere [3]. Figure 1a presents the total detected charge (Z_{tot}) of identified particles as a function of the total detected pseudo parallel linear momentum normalized to the beam one, for 95 A.MeV beam energy. The bidimensional plot 1a) can be divided in two regions which reflect the response of the detector.

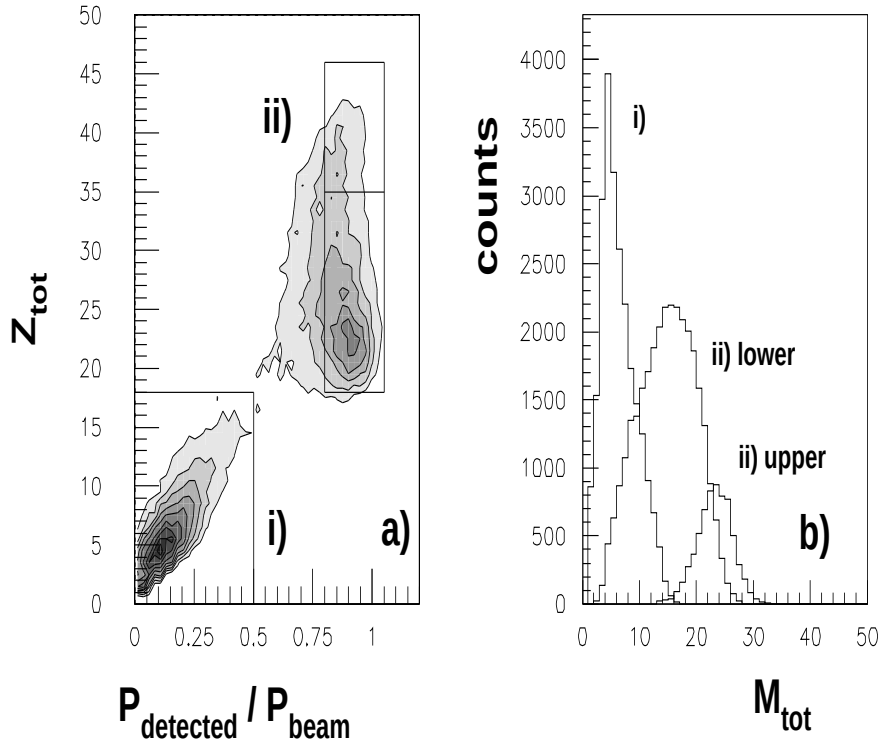

Figure 1: *The relative "pseudo parallel momentum " $P_{detected}/P_{beam}$ versus total charge Z_{tot} is presented in figure a). The total charged particle multiplicity distributioons for the region i), lower part of region ii) and the upper part of region ii) are presented in figure b).*

- the region i) corresponding to the low Z_{tot} and low $P_{detected}$ is associated with peripheral reactions, both the projectile-like and target-like fragments remain undetected because of threshold (target-like) and angular efficiency (projectile-like) effects. The detected charge presents a linear behavior against the detected pseudo parallel linear momentum.

- as soon as the projectile-like fragment is measured, the detected pseudo parallel linear momentum comes close to the projectile one. The frame ii) in the figure 1a) localizes these events. When the projectile-like and target-like fragments are identified the amount of information is complete.

The true "well detected" events are situated in the upper part of ii) but they correspond to a restricted range of central impact parameters. On the other side, to study the evolution of the reaction mechanisms with centrality, we would like to sample events in a large range of impact parameters. Assuming for region ii) that the missing mass and the missing momentum are associated with only one fragment (the target-like residue), conservation laws are used to improve the completeness of region ii). Finally, our definition of "well detected" events corresponds to the region ii) after target-like reconstruction. This corresponds to 40 % of all recorded events with multiplicity ≥ 3. Figure 1b) presents the total charged particles multiplicity M_{tot} for the region i), the lower part of ii) and the upper part of ii).

3 The tool box

For most collisions, peripheral as well as central, the reaction mechanisms are predominantly binary with a quasi-target and a quasi-projectile fragment. The collision can be best investigated in the center of mass of the reaction. To this end, we calculate the following tensor

$$T_{ij} = \sum_{n=1}^{M_{tot}} \frac{P_i^{(n)} P_j^{(n)}}{2m_n}$$

where $P_i^{(n)}$, $P_j^{(n)}$ are the i^{th} and j^{th} cartesian coordinates $(i, j = 1, 2, 3)$ of the charged product momentum $P^{(n)}$, with mass m_n (the masses when not experimentally measured, have been deduced from the Z-identification assuming that the nuclei are produced in the stability valley). The diagonalization of this symmetric tensor gives three eigenvectors associated with three normalized eigenvalues Q_1, Q_2, Q_3 with $Q_1 < Q_2 < Q_3$ and $Q_1 + Q_2 + Q_3 = 1$. The eigenvector corresponding to the largest eigenvalue (Q_3) defines the deflection angle Θ_{flow} relative to the beam axis. This transformation is invariant under clusterisation [4]. The hypothesis of attributing all the missing mass to only one fragment does not influence the deflection axis determination. Therefore the analysis will be performed in the frame defined by the deflection angle Θ_{flow}.
We have chosen to relate centrality to the asymptotic shape of the events. This is done using the second Fox-Wolfram moment H_2, [5] given by the relation:

$$H_2 = \frac{1}{\sum_{m,n}^{M_{tot}} \mid \vec{P_m} \parallel \vec{P_n} \mid} \sum_{m,n}^{M_{tot}} \mid \vec{P_m} \parallel \vec{P_n} \mid \frac{(3cos^2\Theta_{m,n} - 1)}{2}$$

where $(3cos^2\Theta_{m,n} - 1)/2$ is the Legendre polynomials of order 2 and $\Theta_{m,n}$ is the relative angle between the velocity vectors of particles m and n. This variable is invariant under rotation and allows a clear shape event analysis : pencil events tend to give $H_2 \approx 1$ and spherical events tend to give $H_2 \approx 0$.

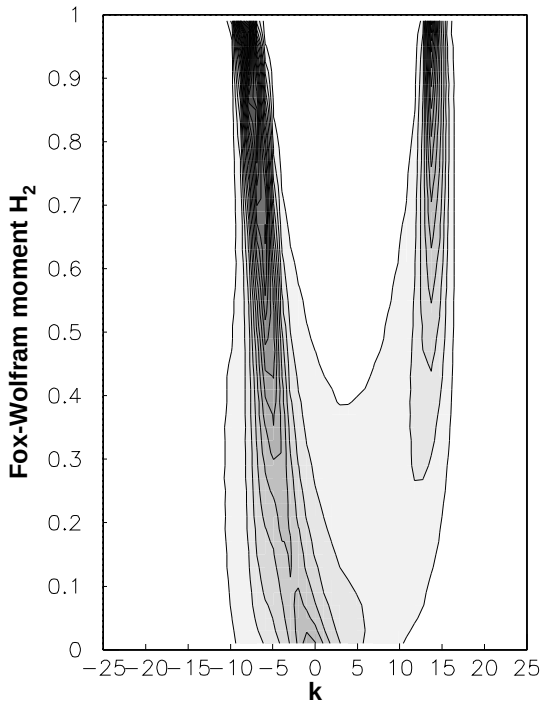

Figure 2: *Isocontour plot (linear scale) of charge density $\rho_Z(k)$ as a function of the bin number k and of the second moment of Fox and Wolfram for Ar + Ni at 95 A.MeV.*

4 Charge density analysis

4.1 Charge density definition

In order to get rid of inevitable multiplicity fluctuations even for a "well detected" event selection, we have calculated the charge density distribution $\rho_Z(k)$ along the deflection axis in the velocity space. To have an axis which is independent of bombarding energy, the velocity axis is divided in k bins with a width $\Delta k = V_{cm}/10$ where V_{cm} is the velocity of the center of mass. With this definition, the center of mass velocity of a particle along this axis is given by $v = k * V_{cm}/10$, where k is the bin number. For the Ar + Ni system at 95 A.MeV, the bins k = -10, 3 and 16 are associated respectively to the target, the nucleon-nucleon and the projectile center of mass velocities. The density distribution along the k axis is then

given by:

$$\rho_Z(k) = \frac{\sum_i Z_i(k)}{\sum_{i=1}^{M_{tot}} Z_i}$$

where the sum in the numerator runs over all charges in bin k, whereas the denominator is the sum of all charges in the whole k-interval considered. The contours $\rho_Z(k)$ in a $H_2 \bigotimes k$ plot are reported in figure 2, for a beam energy of 95 A.MeV. The binary source behaviour is easily recognized for $H_2 > 0.2$. For the most violent collisions, the separation between two sources is not clear and can correspond to "incomplete fusion" events as well as to very damped binary collisions. When two sources are clearly resolved ($H_2 > 0.2$), a charge abundance is observed between the two sources which increases with decreasing H_2 values. This production excess may result from different mechanisms [6]:
-direct emission of particles,
-emission from the outgoing partners on a time scale short enough to preserve some memory effects in the emission kinematics,
-emission resulting from a composite system formed by the overlap between the projectile and the target.

4.2 Filtering method

In order to sort out these different contributions, we construct a filter for the recorded sample. As a first step, the charge density distribution is expressed in term of a development in Hermite polynomials as following:

$$\rho_Z(k) = \sum_{\ell=0}^{\infty} C_\ell(k_0) H_{er}^\ell(k - k_0)$$

$H_{er}^\ell(k - k_0)$ are the usual Hermite polynomial of order ℓ, k_0 the scanning variable and the $C_\ell(k_0)$ are given by:

$$C_\ell(k_0) = \frac{1}{\ell!(2\pi)^{1/2}} \int_{-\infty}^{+\infty} \rho_Z(k_0) e^{-k_0^2/2} H_{er}^\ell(k_0) dk_0 \sim \frac{1}{\ell!(2\pi)^{1/2}} \sum_{k_0} \rho_Z(k_0) e^{-k_0^2/2} H_{er}^\ell(k_0) \Delta k_0$$

Then we build a filter based on the coefficient $\Lambda_{04}(k_0) = C_0(k_0)) - C_2(k_0) + C_4(k_0)$. This linear combination is constructed to maximize the $\Lambda_{04}(k_0)$ value for a Dirac charge distribution of the form $\rho_Z(k) = \delta(k - k_0)$.
The values of the $C_\ell(k_0)$ and $\Lambda_{04}(k_0)$ coefficients are given in table I as a function of hte scanning variable k_0 for two ideal charge distributions.

- A Dirac charge distribution in the central bin,
- Two Dirac charge distributions located respectively at k = -6 and k = 3.

	$C_0(k_0=0)$	$C_2(k_0=0)$	$C_4(k_0=0)$	$C_{odd}(k_0=0)$	$\Lambda_{04}(k_0=0)$
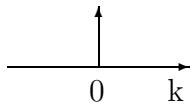	1.0	-0.5	0.125	0.0	1.625
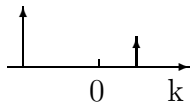	0.0	0.0	0.0	0.0	0.0
	$C_0(k_0=3)$	$C_2(k_0=3)$	$C_4(k_0=3)$	$C_{odd}(k_0=3)$	$\Lambda_{04}(k_0=3)$
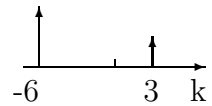	1.0	-0.5	0.125	0.0	1.625
	$C_0(k_0=-6)$	$C_2(k_0=-6)$	$C_4(k_0=-6)$	$C_{odd}(k_0=-6)$	$\Lambda_{04}(k_0=-6)$
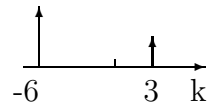	1.0	-0.5	0.125	0.0	1.625

Table I : Values of the $C_\ell(k_0)$ and Λ_{04} coefficients as a function of the scanning variable k_0 for two ideal charge distributions.

For these two ideal cases, the odd $C_\ell(k_0)$ coefficients are always zero by Hermite polynomial transform definition. When the picture evolves from pure two-body to a pure one-body process the coefficient Λ_{04} increases from 0 to 1.625. Due to the finite width of the charges distribution this last asymptotic value is never reached and the C_ℓ for odd ℓ values are not exactly 0.
The correlation between H_2 and $\Lambda_{04}(k_0=0)$ is shown in figure 3 at 32 and 95 A.MeV beam energies. Effectively large $\Lambda_{04}(k_0=0)$ values are then associated with small H_2 values which indicate "spherical" event shapes. The $\Lambda_{04}(k_0=0)$ values near zero are strongly correlated with elongated events ($H_2 > 0.4$).
At 32 A.MeV, the island which corresponds to large $\Lambda_{04}(k_0)$ values is associated with a charge accumulation in the bin $k_0 = 0$ ($V = V_{cm}$). It may be attributed to a single source through "incomplete fusion".

4.3 Scanning

The filtering method, built up to select event configurations with an important charge density for different k_0, can be used to scan the whole velocity region by changing the k_0 values (k_0

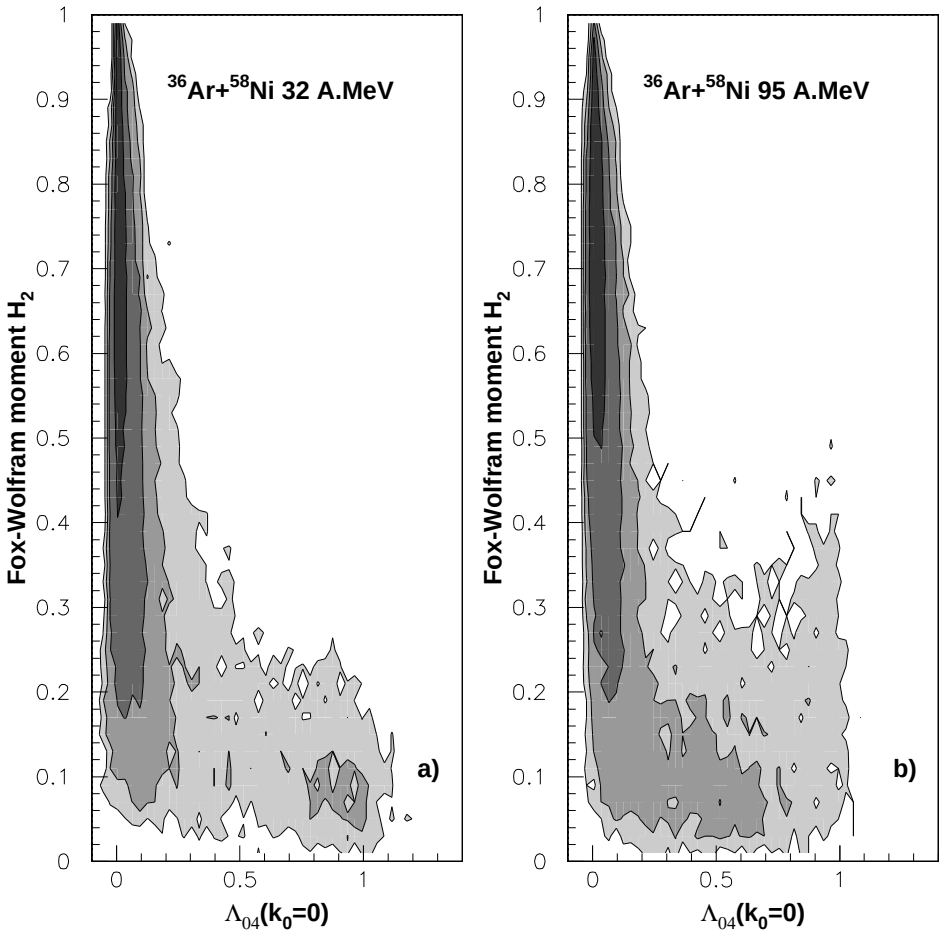

Figure 3: *The correlation between H_2 and $\Lambda_{04}(k_0 = 0)$ is shown for beam energies of 32 and 95 A.MeV. The isocontours are in logarithmic scale.*

= ..., -2, -1, 0, 1, 2, ... positive and negative k_0 values correspond respectively to a right and left shift of the filter central position). This is illustrated in figure 4 for three bins in H_2. The first row shows the charge density distributions as a function of k. The *r.m.s.* values indicated by error bars, are very large. This is due in part to the fact that the charge density is not continuous (presence of clusters). The second row in figure 4 presents the variation of $\Lambda_{04}(k_0)$ with k_0. It is strongly correlated with the charge distribution. It has to noticed that the Hermite transform reduces the fluctuations observed in the charge density distribution. The last row gives the evolution of the coefficient $C_1(k_0)$ as a function of k_0. This coefficient passes through zero with the maximum values of $\Lambda_{04}(k_0)$ distribution, thus permitting a precice "source" localization in spite of the remaining fluctuations in the charge density.

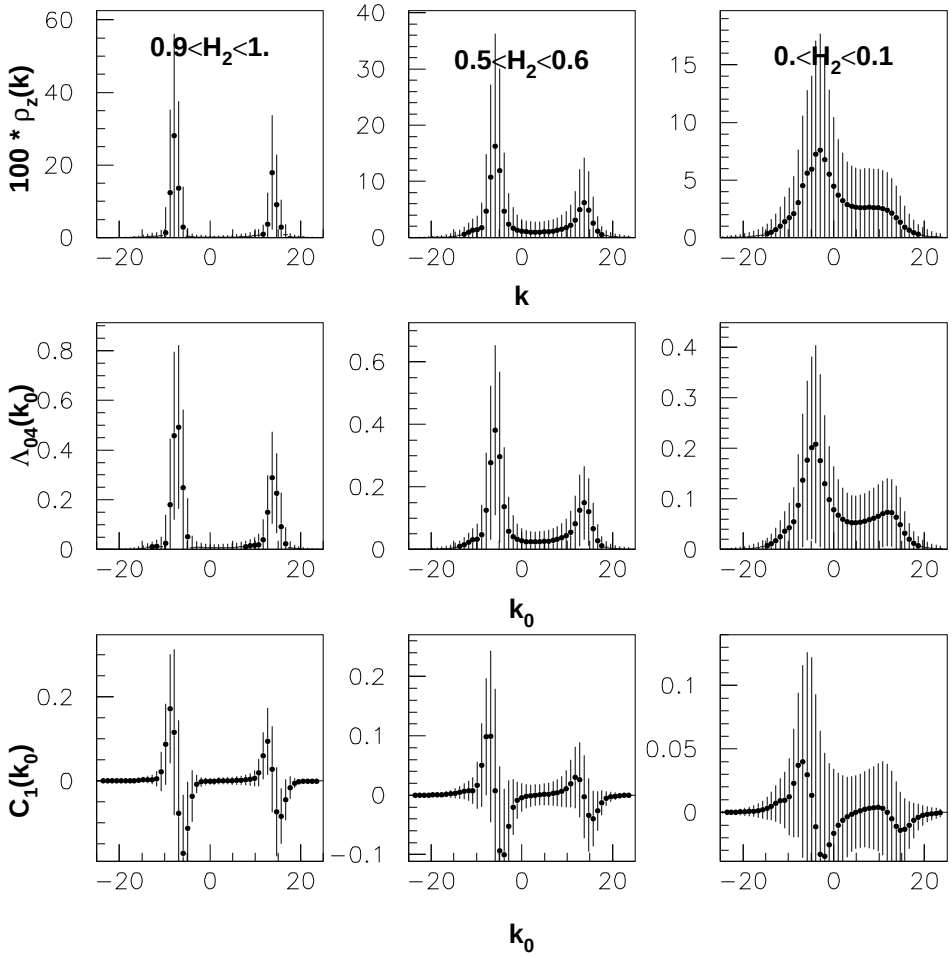

Figure 4: *The first row presents the charge density distributions for three H_2 bins, the second row shows the $\Lambda_{04}(k_0)$ distributions and the third row presents $C_1(k_0)$ distributions.*

5 Applications of the charge density analysis

5.1 Configuration selection

From the above considerations, in order to select events with an rather large charge density between the target-like and the projectile-like fragments, we require that $\Lambda_{04}(k_0 = 3)$ greater than 0.05 with $k_0 = 3$ corresponding to the nucleon-nucleon center of mass velocity. The result of this filtering is illustrated by figure 5. We indeed observe an accumulation of charge around the selected velocity which increases with decreasing H_2 values. Thus, by using an appropriate filter to the charge density in conjunction with the global variable H_2, it is

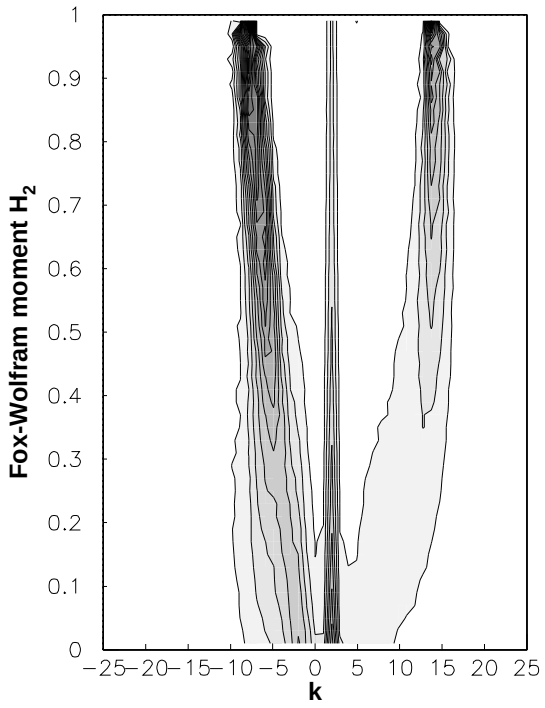

Figure 5: *Isocontour plot (linear scale) of charge density $\rho_Z(k)$ as a function of the bin number k and of the second moment of Fox and Wolfram with $\Lambda_{04}(k_0 = 3) > 0.05$ for the Ar + Ni at 95 A.MeV.*

possible to select well defined event configuration and to visualize the reaction mechanisms.

5.2 Comparison between experimental data and the BNV prediction for the charge density

An extra advantage of this powerful technique is that it allows a direct and quantitative comparison between multidetector fragmentation N-body data and predictions of one-body transport models as BNV, which is a numerical simulation of the nuclear Boltzmann transport equation [7]. In this model one calculates the space time evolution of the one-body distribution function under the influence of the mean field, the nucleon-nucleon collisions

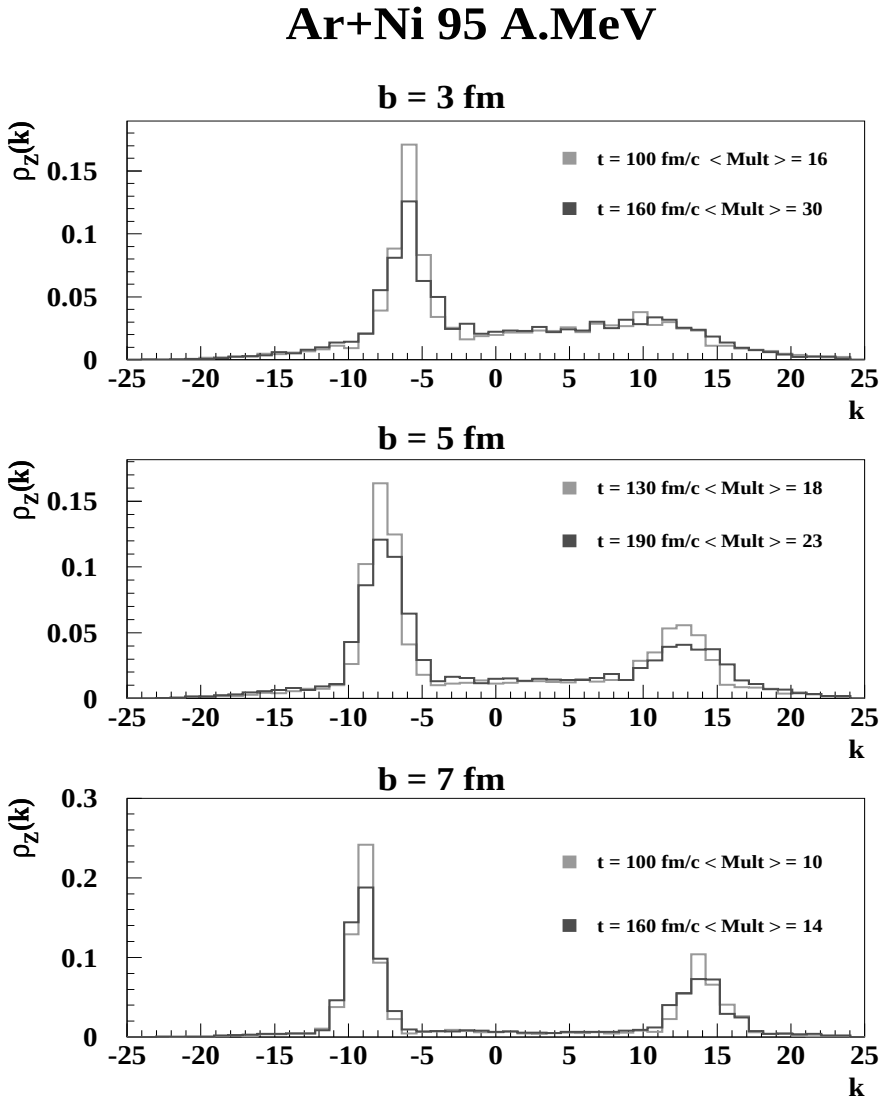

Figure 6: *Charged density distributions for different impact parameters: the predictions of a BNV simulation are shown for different asymptotic times and the corresponding mean charged particle multiplicities (Mult) are indicated.*

and the Pauli principle. In order to compare experimental data and theoretical simulations of Boltzmann type, the commonly used procedure is to calculate N-body variables in the model. For this purpose, the calculation has to be stopped at a freeze-out time when the entrance dynamics is achieved. At this time, fragments are defined through a coalescence prescription and the secondary decay can be taken into account by coupling the calculation to an evaporation or multifragmentation code. The problem with this approach is that the coalescence algorithm contains uncontrollable free parameters. Moreover the definition itself of a freeze-out stage seems to be highly questionable in the Fermi energy regime where the

dynamical and thermodynamical time scales are not well separated.
We propose an alternative method to compare N-body experimental variables with one-body theories. It consists in constructing one-body variables like the charge density defined above for the data as well as for the theory. The absence in the model of multifragment emission exit channels is not important since charge density is by definition multiplicity invariant (as long as Coulomb distorsions are negligible [8] as estimated for this light system), therefore the calculation has to be done up to an asymptotic time (in principle infinite) where nuclear dynamics as well as secondary evaporation are over. Once again multiplicity invariance of the charge density implies that the distributions are independent of the asymptotic time chosen provided it is long enough. This is demonstrated in figure 6 where the BNV predictions for the charge density are presented at different times and different impact parameters. In this way, the calculation can proceed up to an asymptotic time, where nuclear dynamics and secondary evaporation are over. However, even for this maximum time, the long range Coulomb correlations are not completely accounted for. Therefore at this time, fragments are formed with a coalescence model and Coulomb correlations are added up to infinity. At the end of the calculation, we obtain simulated events which in principle could be treated as experimental events. But one has to stress that the clusterization procedure is here just a trick to subtract Fermi motion from the asymptotic one-body distribution function and completely account for Coulomb correlations. For further details about the calculation, see reference [8].
In figure 6, the height of the quasi-projectile and quasi-target peaks is slightly modified by increasing time, reflecting the relative long time scale of the last evaporative steps, but the population at mid-rapidity as well as the localisation in velocity space of the peaks is remarkably constant, showing that a detailed and quantitative comparison with data is possible [8].

6 Conclusions

The charge density variable is used to describe heavy ion reaction in the Fermi energy domain. This variable is robust and digital filtering can be applied. As a result of the filtering, the $\Lambda_{04}(k_0)$ distribution, which gives a smooth picture of the charge density distribution, becomes regular enough to be efficiently handled by an algorithm searching for maxima associated with $C_1(k_0)$ zero values and estimating the integral charge over the associated bumps through the scanning. As a consequence the charge density appears to be a powerful tool for visualization, for configuration selection and finally for the comparison between experimental data and mean field theories.

References

[1] L.P. Csernai,G. Fài and J. Randrup, Phys. Lett. **B140**, 149 (1984).

[2] A. Angot Complément de Mathématiques Masson, Paris(1982).

[3] J. Pouthas et al., Nuc. Inst. Meth, A **357** (1995) 418.

[4] J. Cugnon and D. L'Hote, Nucl. Phys. A **397** (1983) 519.

[5] G.C Fox and S. Wolfram, Nucl. Phys. B **149** (1979) 413.

[6] T. Lefort et al , submitted to publication in NPA.

[7] A. Bonasera, F. Gulminelli, J. Molitoris, Phys. Rep. **243** (1994) 1.

[8] E. Galichet, PhD thesis **Lyon 085-98** (1998).
E. Galichet et al. **in preparation**.